Article

Cite This: Biomacromolecules 2018, 19, 2795−2804

pubs.acs.org/Biomac

Inverse Thermoreversible Mechanical Stiffening and Birefringence in a Methylcellulose/Cellulose Nanocrystal Hydrogel

Ville Hynninen,[†] Sami Hietala,[§] Jason R. McKee,[⊥] Lasse Murtomäki,[∥] Orlando J. Rojas,[†,‡] Olli Ikkala,*[,†,‡] and Nonappa*[,†,‡]

[†]Department of Applied Physics, School of Science, Aalto University, P.O. Box 15100, FI-00076 Espoo, Finland

[§]Department of Chemistry, University of Helsinki, P.O. Box 55, FI-00014 HY Helsinki, Finland

[⊥]Betulium Ltd., Tekniikantie 2, FI-02150 Espoo, Finland

[∥]Departments of Chemical and Metallurgical Engineering and Chemistry and Materials Science, School of Chemical Engineering, Aalto University, P.O. Box 16300, FI-00076 Espoo, Finland

[‡]Department of Bioproducts and Biosystems, School of Chemical Engineering, Aalto University, P.O. Box 16300, FI-00076 Espoo, Finland

Supporting Information

ABSTRACT: We show that composite hydrogels comprising methyl cellulose (MC) and cellulose nanocrystal (CNC) colloidal rods display a reversible and enhanced rheological storage modulus and optical birefringence upon heating, i.e., inverse thermoreversibility. Dynamic rheology, quantitative polarized optical microscopy, isothermal titration calorimetry (ITC), circular dichroism (CD), and scanning and transmission electron microscopy (SEM and TEM) were used for characterization. The concentration of CNCs in aqueous media was varied up to 3.5 wt % (i.e, keeping the concentration below the critical aq concentration) while maintaining the MC aq concentration at 1.0 wt %. At 20 °C, MC/CNC underwent gelation upon passing the CNC concentration of 1.5 wt %. At this point, the storage modulus (G') reached a plateau, and the birefringence underwent a stepwise increase, thus suggesting a percolative phenomenon. The storage modulus (G') of the composite gels was an order of magnitude higher at 60 °C compared to that at 20 °C. ITC results suggested that, at 60 °C, the CNC rods were entropically driven to interact with MC chains, which according to recent studies collapse at this temperature into ring-like, colloidal-scale persistent fibrils with hollow cross-sections. Consequently, the tendency of the MC to form more persistent aggregates promotes the interactions between the CNC chiral aggregates towards enhanced storage modulus and birefringence. At room temperature, ITC shows enthalpic binding between CNCs and MC with the latter comprising aqueous, molecularly dispersed polymer chains that lead to looser and less birefringent material. TEM, SEM, and CD indicate CNC chiral fragments within a MC/CNC composite gel. Thus, MC/CNC hybrid networks offer materials with tunable rheological properties and access to liquid crystalline properties at low CNC concentrations.

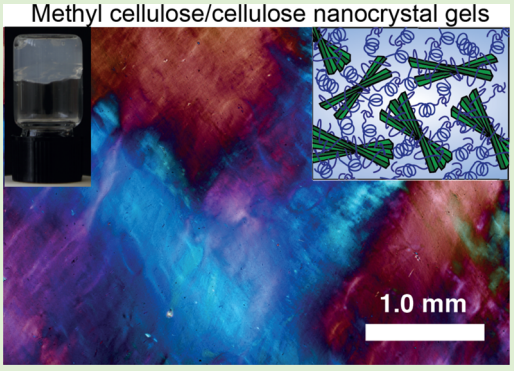

1. INTRODUCTION

Cellulose nanocrystals (CNCs) are rodlike, sustainable nanoparticles that can be extracted from wood and plant-based materials by strong acid hydrolysis.[1] Because of the negative surface charges caused by sulfate half-ester residues from the sulfuric acid hydrolysis (Figure 1a), CNCs form stable aqueous colloidal suspensions that are isotropic at low concentrations.[2−4] However, because of their high aspect ratio (typically 10−50), lyotropic liquid crystalline (LC) order emerges when a critical concentration is exceeded, ≥4−5 wt % in the case of cotton-based CNCs.[3,5,6] The LC assembly is left-handedly twisted and driven by the stacking of the inherently right-handed CNCs and can be detected by optical birefringence via polarized optical microscopy (POM) and optical probes.[3,7−9] The chiral nematic pitch and critical concentration can be tuned, for example by adjusting the electrostatic environment of the CNC or through polymer grafting.[10−14] The cholesteric structure is retained in dried CNC films, which broadens the scope for possible CNC-based photonic, plasmonic, and composite material applications.[8,15−21]

Because of their excellent mechanical properties, aspect ratio, low density, tunable surface chemistry, and biocompatibility, CNCs have been studied as fillers and reinforcing additives in a variety of compositions ranging from cement paste to composite fibers and hydrogels.[22−32] Additionally, pristine CNCs form gels at sufficiently high concentrations or when suitably modi-

Received: March 5, 2018
Revised: May 6, 2018
Published: May 7, 2018

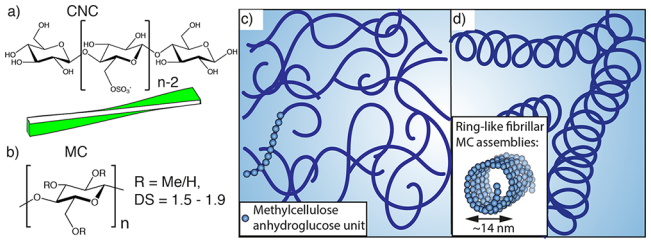

Figure 1. Components of the composite hydrogel: The chemical structures of (a) cellulose nanocrystal (CNC) showing the repeat units with a scheme of the colloidal rod and (b) methyl cellulose (MC). (c) At 20 °C, aq MC behaves as individual polymer chains. (d) At 60 °C, the aq MC chains are supramolecularly aggregated into shape-persistent fibrillar assemblies with hollow ring-like lateral structure.[47−52]

fied.[5,6,33] However, for their effect to be maximized, it is important to control their assembly over several length scales.[34,35] Therein, both the LC assembly of CNCs and the interactions with the surrounding matrix are crucial. The packing of CNCs has been studied in detail in confined spaces by capturing CNC suspensions in microdroplets.[36−39] By tuning the solvent concentrations and evaporation, the LC morphologies within the dried spheres have been effectively controlled.[36,38] Additionally, by infusing nanoparticles into the droplets, plasmonic, fluorescent, and magnetic properties have been achieved, which has given further insight into the interactions within the cholesteric CNC phase.[37]

On the other hand, methylcellulose (MC, Figure 1b) has attracted considerable interest due to its biocompatibility and ability to form thermosensitive gels.[40−46] It has been shown that, upon heating, the MC chains in aqueous solutions aggregate into persistent fibrils with a hollow, ring-like lateral structure of ∼14 nm diameter and length of several hundreds of nanometers.[47−52] In water at room temperature (20−22 °C), MC chains exist in the form of random coils (Figure 1c,d).[52]

Recently, applications combining the properties of CNCs and MC have been pursued, encouraged by the biocompatibility of both components and that their composite gels allow tunable materials.[41,44,53−55] In particular, the aqueous dispersion of methyl cellulose displays inverse thermoreversible properties, ii.e., the free-flowing aqueous dispersion of MC (at room temperature) undergo gelation upon heating (above 40 °C) in a reversible manner (sol ↔ gel transition). Inverse thermoreversibility has been observed also in other systems.[56] The MC/C hybrids form composite hydrogels that, upon heating from room temperature to 60 °C, display a reversibly increased storage modulus.[32] They also form MC/CNC nanocomposite aerogels[57] and latexes with a double morphology.[58] Several hypotheses have been proposed in the literature, suggesting that MC fibers colloidally wrap the CNCs.[58,59] However, more detailed investigations of the complex interactions and assemblies formed by MC/CNC hydrogel systems have remained unexplored.

In this work, a systematic investigation of mechanical, optical, and morphological details of MC/CNC hydrogels is carried out using multiple complementary techniques. The interplay of rheological and optical (birefringence) properties are studied at room temperature and upon reversible heating from 20 °C to 60 °C by keeping a fixed aq MC concentration at 1.0 wt % and varying the aq CNC concentration up to 3.5 wt %. The incorporation of CNC rods in a MC hydrogel above a certain concentration, and especially upon heating to 60 °C, would modify the rheological properties and optical birefringence due to the inverse thermoreversible nature of MC. The interactions between MC and CNC are explored at room and higher temperatures via isothermal titration calorimetry (ITC). The combination of rheology, quantitative birefringence studies, electron microscopy, and ITC offers new insights into the complex behavior of the MC/CNC hydrogels.

2. EXPERIMENTAL SECTION

2.1. Materials. Methylcelluloses (MCs) with different molecular weights of 14,000 g/mol (product no. M7140, lot# SLBQ9046V), 41,000 g/mol (product no. M0262, lot# SLBR8963V), and 88,000 g/mol (product no. M0512, lot# 079K0054V), hereafter abbreviated as MC14, MC41, and MC88, respectively, were purchased from Sigma-Aldrich. All MC polymers had a methoxy substitution between 27.5 and 31.5% (weight) and a degree of substitution of 1.5−1.9 to produce maximum water solubility as reported by the supplier. Whatman grade 1 qualitative filter papers (cat no. 1001 125), Whatman grade 541 hardened ashless filter papers (cat no. 1541-125, lot# 9722517), and Spectra/Por 1 standard regenerated cellulose dialysis tubing with molecular weight cutoff of 6−8 kDa (part no. 132665, lot# 9200679, Spectrum Laboratories, Inc.) were purchased from VWR. Sulfuric acid (95−97%, product no. 1.00731, lot# K47798131) was bought from Sigma-Aldrich and used as received. Ultrapure Milli-Q water (18 mΩ) was used in all experiments.

2.2. Cellulose Nanocrystals (CNCs). CNCs were prepared from Whatman grade 1 filter paper following the procedure of Edgar and Gray.[60] The filter paper sheets were mechanically ground with a Wiley Mini-Mill (Thomas Scientific, USA) equipped with size 30 filtering mesh to produce homogeneous powder. The resulting powder was hydrolyzed with 64% sulfuric acid. Typically, 272.3 g of sulfuric acid (95−97%) was slowly mixed into 136.2 g of MQ H_2O to produce the desired concentration. The acid solution was allowed to cool to room temperature before proceeding. Fifteen grams of paper powder was weighed into a 500 mL round-bottomed flask followed by the addition of 64% sulfuric acid solution. The mixture was manually agitated with a glass rod until the paper powder was wetted and submerged into the acid solution. The flask was set into a 45 °C water bath and equipped with a Teflon stirring arm, and the paper powder was hydrolyzed under gentle mechanical stirring (32 rpm) for 45 min at 45 °C. The reaction was stopped by pouring the reaction mixture into 3 L of MQ H_2O, i.e., by diluting it ∼10-fold, and it was then left to sedimentate for 20 h. The clear supernatant was discarded by decanting, and the remaining cellulose suspension was washed twice by centrifugation in the following sequence: first, at 6000 rpm for 20 min (Wifug X-3 centrifuge with a fixed angle rotor) and then at 2500 rpm for 45 min, both under ambient conditions. After each centrifugation, the supernatant was discarded by decanting, and the pellet was redispersed in MQ H_2O. A glass rod was used to homogenize the larger aggregates. The CNC dispersion was further purified by dialysis against MQ H_2O until the conductivity of the dialysate stayed below 5 μS/cm. Finally, the CNC dispersion was filtered through Whatman 541 filter paper and stored at +4 °C until use. Stock solutions containing a 3.5 wt % (35 mg/mL) CNC dispersion were prepared through slow evaporation of water by placing the dispersion in a beaker on a heated magnetic stirrer plate at 250 rpm and 45 °C. The solid content of the CNC dispersion was determined gravimetrically by pipetting 1 mL of the dispersion on a watch glass of known weight and placing the watch glass in an oven at 70 °C for 20 h to evaporate water and then reweighing the watch glass.

2.3. MC/CNC Composite Hydrogels. MC−CNC gels were prepared following a previously reported procedure.[32] CNC stock dispersion (3.5 wt %) was first diluted to the desired concentrations ranging from 0.5 to 3.5 wt % using MQ H_2O in volumes close to 10 mL in 40 mL glass vials. An appropriate amount of dry MC powder was then added to the CNC dispersion to obtain the desired concentration. The mixture was first manually agitated to ensure the dispersion and wetting of MC and then further stirred and dissolved by magnetic stirring (250 rpm) for 48 h under ambient conditions. The as-prepared gels were stored in a refrigerator at 4 °C (at least 20 h) until use.

DOI: 10.1021/acs.biomac.8b00392
Biomacromolecules 2018, 19, 2795−2804

2.4. Dynamic Light Scattering (DLS) and Zeta Potential (ζ). DLS and zeta (ζ) potential measurements were performed with a Zetasizer Nano ZS90 (Malvern Instruments). Twelve mm square polystyrene cuvettes (product no. DTS0012, Malvern Instruments) were used for DLS, and folded capillary zeta cell cuvettes (product no. DTS1070, Malvern Instruments) were used for zeta potential measurements. Samples of MC88 0.25 wt %, CNC 0.5 wt %, and MC/CNC mixtures with the following compositions 0.25/0.25, 0.25/0.5, and 0.5/0.5 (wt %/wt %) were used for ζ-potential measurements. All samples contained 1.0 mM of NaCl. For hydrodynamic size distribution, more dilute samples of MC 0.1 wt %, CNC 0.2 wt %, and MC/CNC 0.1 wt %/0.1 wt % were used. The samples were prepared as described above for MC/CNC hydrogels. The reported distributions and values are the average of three measurements.

2.5. Conductometric Titration. The sulfate group content of CNCs was determined using a conductometric titrator 751 GPD Titrino (Methrom AG) together with Tiamo software as described in the literature.[61] Before the titration, the sulfate groups on CNCs were protonated by adding concentrated hydrochloric acid (HCl) to the CNC dispersion so that the final HCl concentration was 0.1 M. The mixture was incubated for 15 min after which the excess acid was removed by dialysis against Milli-Q water until the conductivity of the dialysate remained below 5 μS/cm. For the titration, 20 mL of the obtained CNC dispersion was added to 490 mL of degassed Milli-Q water followed by addition of 0.5 mL of 0.1 M HCl and 1.0 mL of 0.5 M NaCl. The resulting dispersion was titrated against 0.1 M NaOH under constant stirring at 300 rpm. Sodium hydroxide (NaOH) solution was added in 0.02 mL increments every 30 s. The acidic sulfate content was calculated as described in the standard procedure (SCAN-CM 65:02) as a ratio of the NaOH (in μmol) required to neutralize the sulfate groups to the amount of CNC (g) in the dispersion.

2.6. Rheological Measurements. Rheological properties of the gels were determined following the procedures reported previously.[32] TA AR2000 stress-controlled rheometer with a 20 mm steel plate−plate geometry and a Peltier heating system was used. Systematic measurements at different CNC concentrations, ranging from 0 to 3.5 wt %, at a fixed concentration of 1.0 wt % of MC88 were performed at 20 or 60 °C. Additionally, samples prepared with 0.5 wt % MC88 concentration and with 1 wt % of MW14 or MC41 combined with 3 wt % of CNCs were measured as reference. Samples were thermally equilibrated for 1 min prior to measurements. Strain-dependent rheological properties were determined at an oscillation frequency of 6.283 rad/s, and frequency sweeps were done at 1% strain at both 20 and 60 °C. The samples were covered with a sealing lid to curtail evaporation during the measurement. For the characterization of cyclic temperature response, the samples were heated from 20 to 60 °C and cooled to 20 °C with an increment of 3.0 °C/min. In the temperature sweeps, the storage modulus (G') and loss modulus (G'') were recorded at an angular frequency of 6.283 rad/s and 1.0% strain.

2.7. Polarized Optical Microscopy (POM). Polarized optical microscopy was performed with Leica DM4500 P high-end polarization microscope combined with a Canon EOS 70D DSLR camera. For studying changes in the temperature-dependent birefringence, MC88/CNC gels were imaged during a 20−70−20 °C temperature cycle with 10 °C increments. The heating rate was of 3 °C/min, and the samples were allowed to thermally equilibrate for 30 s before acquiring each image. A Linkam LTS 350 heating stage together with TMS 94 temperature programmer and LNP liquid nitrogen pump (Linkam Scientific Instruments, United Kingdom) were used for temperature control. Fixed, identical microscope and camera settings were used for all samples to allow the quantification and comparison of the birefringence intensities. The constant settings were first determined based on the sample with the highest concentration (MC88/CNC 1.0 wt %/3.5 wt %), which presented the maximum birefringence to avoid saturation of the images. The birefringence intensity was then determined as the image mean intensity value using ImageJ.[62,63] The gel samples were prepared by placing the sample material inside a SecureSeal imaging spacer (Grace Bio-Laboratories inc., USA) attached on a microscope glass slide, which was then covered with a cover glass. Samples with MC14 and MC41 were imaged under similar conditions for reference purposes. For acquiring colored images, in addition to crossed polarizers, a full-wave plate was used for enhanced colors.

2.8. Transmission Electron Microscopy (TEM). TEM imaging of CNCs and MC88/CNC gels was performed with a JEM-2800 (JEOL) high-resolution TEM microscope operating at 200 kV. Gel samples were prepared on plasma cleaned (30 s, Gatan Solarus 950) and preheated (65 °C) C-flat 200 mesh copper grids with holey carbon support film (Electron Microscopy Sciences). Dilute MC/CNC dispersions (MC88/CNC 0.3 wt %/0.0 and 0.3 wt %/0.3 wt %) were prepared and heated to 65 °C for 15 min. Three microliters of gel was then pipetted onto the TEM grid, gently blotted with filter paper edge, and allowed to dry completely at 65 °C. For samples prepared at room temperature, 3 μL of gel was then pipetted onto the TEM grid, gently blotted with filter paper edge, and allowed to dry under ambient conditions for 24 h. Plasma-cleaned 300 mesh copper grids with carbon-only support film (Electron Microscopy Sciences) were used for the CNC samples. Ten microliters of dilute CNC solution was pipetted onto the grid, incubated for 1 min at RT, and then blotted with filter paper.

2.9. Scanning Electron Microscopy (SEM). SEM imaging was performed with a Zeiss Sigma VP scanning electron microscope at 1−1.5 kV acceleration voltage. For sample preparation, a droplet of ∼10 μL of MC88/CNC mixture was pipetted on an aluminum SEM stub with carbon tape. The sample was frozen by plunging it in liquid propane for 45 s and then transferring it into liquid nitrogen for at least 5 min and then freeze-dried in a vacuum overnight to obtain aerogels. Alternatively, 200 μL of sample material was directly pipetted into a 1.5 mL microcentrifuge tube and frozen by immersing in liquid nitrogen for 5 min and then freeze-dried in a lyophilizer (0.016 mbar, −100 °C) for 20 h. The aerogel samples were attached on aluminum SEM stubs with carbon tape and coated with 5 nm of gold−palladium by using a Leica EM ACE600 high vacuum sputter coater prior to imaging.

2.10. Circular Dichroism Spectroscopy. Circular dichroism (CD) spectra were recorded from MC/CNC gels of various compositions (MC 1.0 wt %, CNC 3.5 wt %, MC/CNC 1 wt %/0.5 wt %, MC/CNC 1.0 wt %/1.5 wt %, and MC/CNC 1.0 wt %/2.5 wt %) by using a Chirascan CD spectrometer (Applied Photophysics) and quartz cuvettes with a 1.0 cm path length. The spectra were measured in the 200−500 nm range using a 0.5 nm step and 0.5 s dwell time. The background was determined from pure Milli-Q H_2O and was automatically subtracted from the sample data.

2.11. Isothermal Titration Calorimetry (ITC). Calorimetric titrations were performed with a MicroCal VP-ITC isothermal titration calorimeter (Malvern Instruments). Briefly, 25 successive 10 μL injections of CNC (0.45 wt %; 0.5 μM, see Supporting Information for the estimation of the molarity of the CNC solution) were added to a reaction cell containing 1.8 mL of MC solution 0.05 mM (0. 44 wt %) of MC88, 0.1 mM (0.41 wt %) of MC41, or 0.3 mM (0.42 wt %) of MC14. For preparation of the sample solutions, CNCs were dialyzed against MQ H_2O until the conductivity of the dialysate was below 5 μS/cm (pH 5.24). The excess dialysis water was then used to prepare the desired MC solutions and to dilute CNC accordingly. All solutions were degassed before the measurements, which were performed at both 25 and 60 °C under constant stirring (307 rpm). At 25 °C, the elapsed time between the successive injections was 360 s and 600 s at 60 °C. Titration heat signals were processed with MicroCal Origin data analysis software. For curve fitting, one set of sites model was applied, and the CNC was assumed to behave as a ligand. The heats of dilution of adding CNC into the dialysis water without MC, at both 25 and at 60 °C, were used as reference and subtracted from the respective measurement runs (see Supporting Information, Figure S1).

3. RESULTS AND DISCUSSION

The morphology, surface charge, and aggregation behavior of freshly prepared CNCs dispersed in aqueous media were characterized with TEM, DLS, and POM. The mean length and width of the CNCs were 181 ± 69 and 7 nm, respectively, as determined from TEM image analysis (see Figure S2a for size distribution analysis), typical for cotton-based CNCs.[64] The CNC ζ-potential was −64 mV (Figures S2b and S3), implying

DOI: 10.1021/acs.biomac.8b00392
Biomacromolecules 2018, 19, 2795−2804

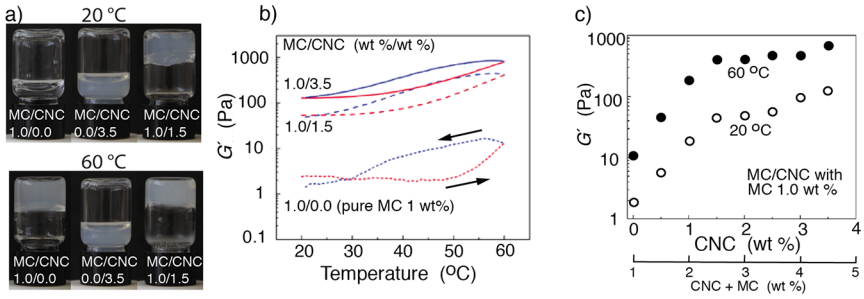

Figure 2. (a) Gelation of aq MC88, CNC, and MC88-CNC composites at 20 and 60 °C as shown by vial inversion. The compositions are given in aqueous wt %. (b) Storage moduli as determined with dynamic rheology of MC88/CNC hydrogels as a function of temperature (b) for three compositions and as a function of CNC concentration (c) for 20 and 60 °C (for comparison, see Figure S9 using the linear G' scale). Note that in (b) and (c), the aq MC concentration is fixed at 1 wt %, and the aq CNC concentration is varied.

excellent colloidal stability due to Coulombic interactions, and the sulfate content was determined by conductometric titration to be 234 μmol/g (see Supporting Information, Figure S4), which is in agreement with previous reports.[58] Polarizing optical microscope (POM) studies of the CNC dispersions showed birefringence at high concentrations, indicating liquid crystalline packing (see Figure S5 for POM images of CNCs at different concentrations), a typical property of sulfuric acid-hydrolyzed CNCs.[3,5,7] As qualitatively shown in Figure 2a, aq MC 1.0 wt % alone remained as a clear/transparent solution at 20 °C (room temperature). Similarly, CNC 3.5 wt % dispersion also remained as a nongelling liquid. However, in the presence of MC (1.0 wt %), aq CNC 0.5 wt % showed a visible change in the appearance, manifesting resistance to flow upon vial inversion, whereas MC/CNC 1.0 wt %/1.5 wt % showed clear gelling. Upon heating to 60 °C, aq MC 1.0 wt % showed gelation (Figure 2a); CNC 3.5 wt % remained as a nongelling dispersion, and MC/CNC 1.0 wt %/1.5 wt % showed strong gelation.

3.1. Dynamic Rheology. The viscoelastic properties of the MC88/CNC hybrid hydrogel were studied by dynamic rheology. The complete rheological data is reported in the Supporting Information, and the core findings are shown in Figure 2b and c for a fixed aq concentration of MC (1.0 wt %) and aq CNC loading from 0 to 3.5 wt % (see Figures S7 for the frequency sweeps at 20 and 60 °C as well as rheological control experiments in Figure S6 for pure CNC). The strain sweeps revealed a linear viscoelastic region up to ~10% strain at 20 °C (Figure S7). Beyond that, a declining storage modulus G' was observed, indicating a slight shear thinning. Ideal viscous fluids are expected to show the storage and loss moduli to scale with the angular frequency as $G' \sim \omega^2$, $G'' \sim \omega^1$ at small ω with $G' \ll G''$, whereas ideal elastic gels are characterized by $G' \sim \omega^0$, $G'' \sim \omega^0$, and $G' \gg G''$.[65] Pure MC88 (1.0 wt %, Figure S7a) shows $G' \sim \omega^{1.7}$, $G'' \sim \omega^{0.9}$, and $G' \ll G''$ at low ω, i.e., viscous fluid behavior, even though not fully ideal. At 20 °C, upon adding CNC, the moduli increased, and their scaling behavior began to indicate a gel-like response. At 60 °C, the rheological behavior was different. Even pure MC (aq 1.0 wt %) displayed gel-like response with $G' = 10$ Pa and $G'' = 2$ Pa. In all MC88/CNC mixtures at 60 °C, G' was clearly higher than G'', both independent of ω, characteristic for elastic gels. The samples also turned turbid upon heating (Figure 2a). At 60 °C, the low strain limit G' values increased from 12 Pa (for MC88/CNC 1.0 wt %/0.0 wt %) to 540 Pa (for MC88/CNC 1.0 wt %/3.5 wt %), i.e., a significant increase. At 60 °C, strain sweeps of the hybrid gels typically showed strain hardening above 30% strain (Figure S7). In general, the elastic moduli were reversibly increased by an order of magnitude due to heating, as depicted in Figure 2b. By adjusting both the CNC concentration and temperature, the storage modulus was in total adjustable from 1.6 Pa (for MC88/CNC 1.0 wt %/0.0 wt % at 20 °C) to 850 Pa (for MC88/CNC 1.0 wt %/3.5 wt % at 60 °C), i.e., over 530-fold increase. Hysteresis was observed in consecutive heating and cooling scans, though the moduli values consistently returned to close to the original values (Figure S8). Figure 2c illustrates that the storage moduli increased steeply until the CNC concentration reached ~1.5 wt % (with MC88 concentration fixed at 1.0 wt %), beyond which a plateau and clear gelation was obtained. This suggests a mechanical percolation phenomenon to be discussed later in the context of birefringence. Altogether, the findings are consistent with the previous rheological studies,[32] and the percolation, not thoroughly recognized thus far, was found relevant to our mechanistic observations. Similar trends were observed for the hybrid gels based on lower molecular weight polymers MC14 and MC41 even though limited to lower moduli (Figure S10).

3.2. Morphology. MC88/CNC hydrogels were imaged by TEM. The pure colloidal CNCs were clearly resolved in TEM (Figure 3a); however, resolving the MC component was challenging. Upon heating to 60 °C, MC aggregates were expected to form fibrillar structures consisting of hollow ring-like structures of 14 nm lateral sizes and lengths of several hundreds of nanometers (Figure 1d).[47−52] Panels b and c in Figure 3 show the TEM micrographs of the MC/CNC 0.3 wt %/ 0.3 wt % sample from 20 and 60 °C, respectively. Low concentration was used to better resolve the components. It shows that the CNC was roughly homogeneously distributed within the MC matrix, even though slight CNC bundling cannot be excluded. We were unable to visualize the MC88 fibrils using TEM. Importantly, no CNC alignment was observed in TEM micrographs excluding nematic CNC order.

Freeze-drying allowed another indirect way to investigate the morphologies. Figure 4 shows some of the representative SEM images of aq MC88, CNC, and MC/CNC gels freeze-dried from 20 or 70 °C. When aq MC88 (1.0 wt %) was freeze-dried from 20 °C using liquid nitrogen, SEM images showed mostly film-like structures with a few fibrillar structures (Figure 4a). In contrast, rapid freezing of MC from 70 °C showed a pronounced tendency for the fibrillar structures (Figure 4b) in addition to formation of sheets. This is not unexpected taken the suggested formation of ring-like hollow persistent fibrillar MC aggregates.[52] Pure CNC also showed sheets upon freeze-drying (Figure 4c,d) with little fibrillar interconnections. On the other hand, when MC/CNC 1.0 wt %/3.5 wt % was freeze-dried from 20 °C, sheet-like

DOI: 10.1021/acs.biomac.8b00392
Biomacromolecules 2018, 19, 2795−2804

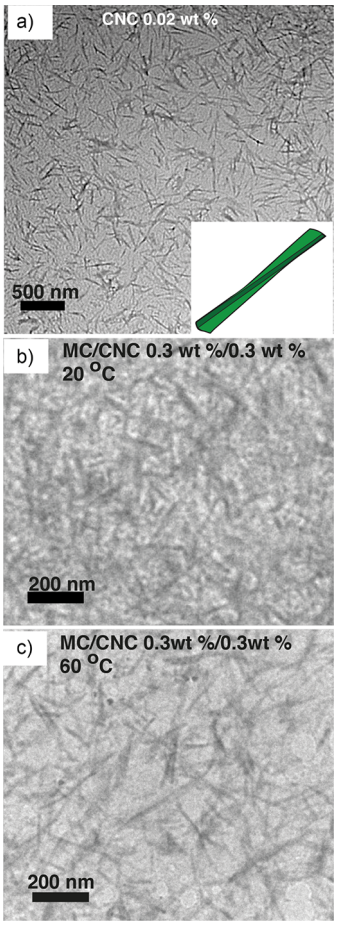

Figure 3. Transmission electron microscopy images. (a) TEM image of CNC 0.02 wt % shows well-dispersed nanocrystals in water at 20 °C. (b) TEM image of MC/CNC 0.3 wt %/0.3 wt % hydrogel at 20 °C. (c) TEM image of MC/CNC 0.3 wt %/0.3 wt % hydrogel at 60 °C.

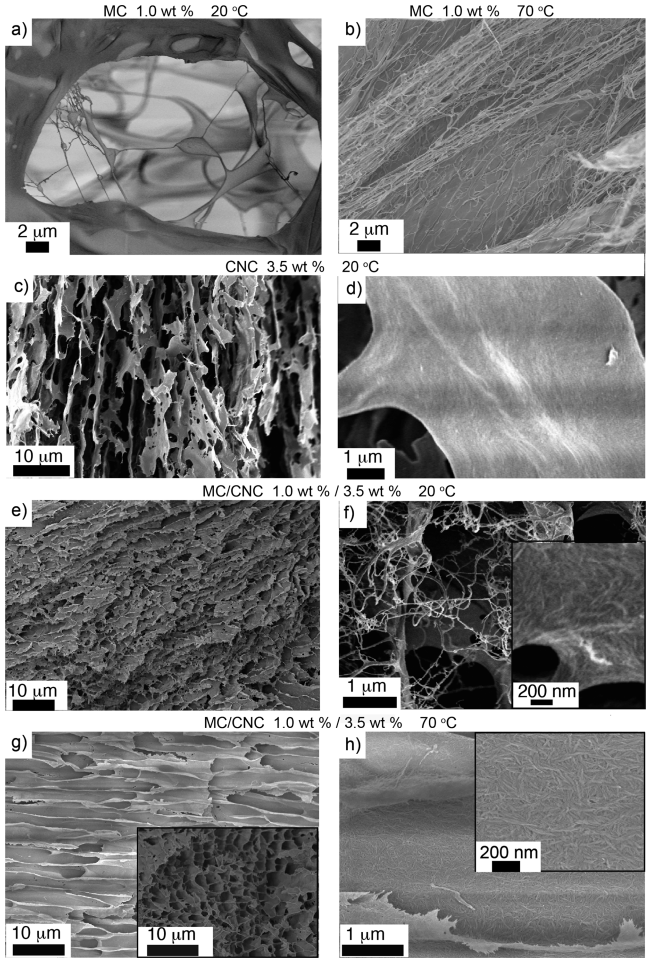

Figure 4. Scanning electron microscopy images of freeze-dried aerogel samples. (a) MC88 1.0 wt % freeze-dried from 20 °C. (b) MC88 1.0 wt % freeze-dried from 70 °C. (c,d) CNC 3.5 wt % freeze-dried from 20 °C. (e,f) MC/CNC 1.0 wt %/3.5 wt % freeze-dried from 20 °C. (g,h) MC/CNC 1.0 wt %/3.5 wt % freeze-dried from 70 °C.

structures were observed that were largely composed of CNCs as a close-up shows random CNC structures (Figure 4e,f).

The sheets were interconnected with MC fibers. The situation further changed for MC/CNC 1.0 wt %/3.5 wt % freeze-dried from 70 °C, which showed well-aligned sheets compared to that at room temperature. The high-resolution SEM images clearly showed that the sheets were composed of CNCs, and few interconnecting fibrils were observed. Important for the subsequent conclusions, high-magnification images of sheets (freeze-dried both 20 and 70 °C) did not suggest any CNC alignments. This indirectly points toward excluding nematic order in MC/CNC in explaining the birefringence. Instead, CNC chiral fragments within the MC gel network would be the natural source of the birefringence to be discussed next.

3.3. Birefringence. POM was used to explore the birefringence and related liquid crystallinity within the MC88/CNC gels. Pristine CNC forms cholesteric liquid crystals in water at sufficiently high concentrations (>4−5 wt %).[5−7] In the present MC88/CNC gels involving low concentrations (<3.5 wt % of CNC, i.e., less than the critical LC concentration for pure aq CNC), liquid crystallinity would not be expected. Therefore, it was not trivial to observe birefringence in the MC/CNC gels at low CNC concentrations, see Figure 5a for MC/CNC 1.0 wt %/2.5 wt %. As a reference, aq MC88 1.0 wt % showed no clear birefringence (Figure 5b). At 20 and 70 °C, clear birefringence was observed in MC88/CNC bicomponent gels for the aq CNC concentrations in the range 1.0−3.5 wt % for the fixed aq MC concentration 1.0 wt %. A surprisingly clear stepwise increase was seen between the CNC concentrations 1.0 and 1.5 wt % at both 20 and 70 °C. However, already for the added CNC concentration of 1.0 wt %, slight birefringence emerged (Figure S11), and at a CNC concentration as low as 0.5 wt %, transient shear-induced birefringence could be detected in MC/CNC hybrid gels, which is an order of magnitude lower concentration compared to what is typical for CNCs alone to exhibit birefringence. The birefringence intensity increased with increasing CNC concentration, and the intensity of MC88/CNC 1.0 wt %/3.5 wt % gel was nearly 2 orders of magnitude higher when compared to the 1.0 wt %/0.5 wt % MC88/CNC gel, for example.

Interestingly, the birefringence critical concentration 1.0−1.5 wt % CNC would also agree with the observed percolation threshold for the storage modulus near 1.5 wt % of CNC for a fixed 1 wt % MC (Figure 2c). Putting this in perspective, CNC-induced order within gels has been observed also in alginate−CNC mixtures,[25] and in a few cases, birefringence has been reported in cellulose nanofiber gels.[66]

It would be natural to expect that the birefringence, i.e., the optical anisotropy, would be reduced upon heating. By contrast, we observed that the birefringence increased upon heating from

DOI: 10.1021/acs.biomac.8b00392
Biomacromolecules 2018, 19, 2795−2804

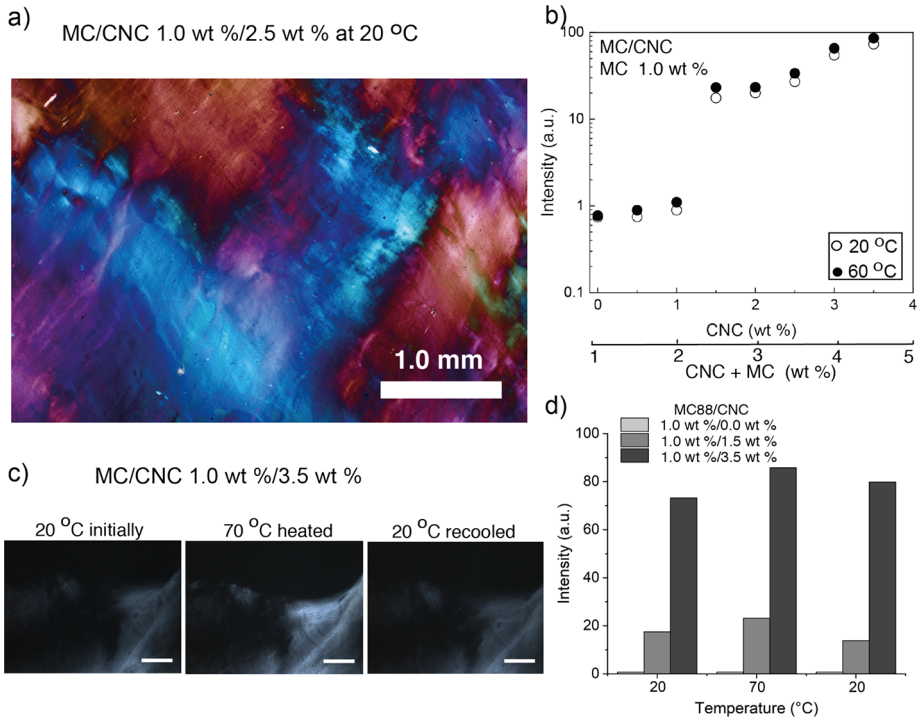

Figure 5. (a) The MC/CNC gels were strongly birefringent as demonstrated by POM imaging of MC88/CNC 1.0 wt %/2.5 wt % at 20 °C. (b) Birefringence as a function of CNC concentration by keeping the concentration MC fixed at 1.0 wt %. Note the stepwise percolative increase of birefringence between 1.0 and 1.5 wt % of CNC. Note the logarithmic scale. (c) POM micrographs of MC88/CNC 1.0 wt %/3.5 wt % at room temperature, upon heating to 70 °C, and upon recooling to room temperature, showing a reversible increase of the birefringence upon heating. Scale bars, 200 μm. (d) Thermoreversible increase of birefringence for three MC/CNC compositions. Note that a linear scale is selected in this case.

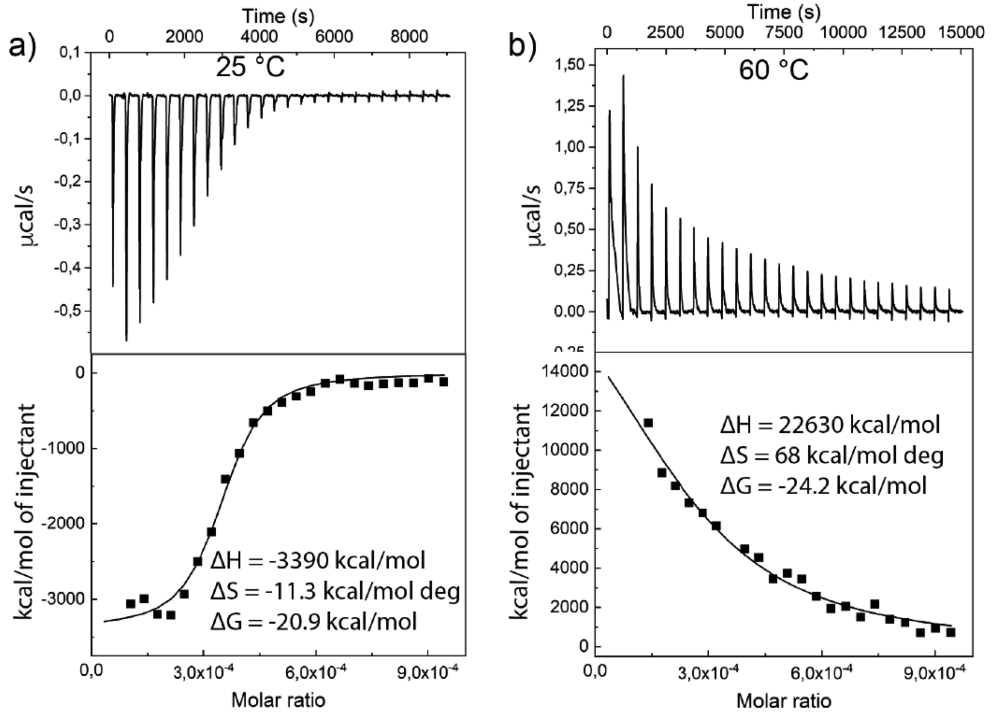

Figure 6. ITC titration curves and respective fits (a) at 25 °C and (b) at 60 °C for MC41/CNC showing that, at room temperature, the MC and CNC components bind enthalpically. By contrast, at 60 °C the entropy dominates, suggesting hydrophobic interactions and structural adjustments, thus promoting CNC packing with the MC gel network.

room temperature to 70 °C and reversibly decreased upon cooling back to room temperature (as qualitatively shown in Figure S12). More quantitatively, the extents of birefringence at different compositions and at 20 and 70 °C are depicted in Figure 5d and Figure S13. The thermoreversible birefringence was reduced for the lower CNC concentrations. Therefore, like the

DOI: 10.1021/acs.biomac.8b00392
Biomacromolecules 2018, 19, 2795−2804

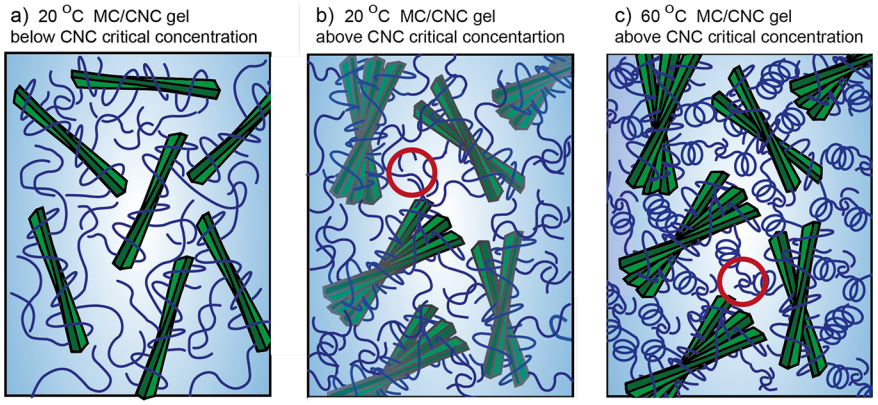

Figure 7. Schematics for the MC/CNC composite gels. (a) Below the CNC critical concentration at 20 °C. (b) Above the CNC critical concentration at 20 °C. (c) Above the CNC critical concentration at 60 °C when the MC chains have the tendency to aggregate into helically winding fibrils. The suggested entanglements within MCs are highlighted with red circles.

rheological properties, birefringence showed inverse thermoreversibility.

Regarding the source of the birefringence, TEM and SEM allow for excluding nematic CNC order. Additional insight was gained from CD spectroscopy of pure CNC, MC, and MC/CNC systems.

The pure CNC (3.5%) showed CD signal at 20 °C, suggesting that, above a certain concentration (i.e., critical CNC concentration), the CNCs exist as chiral aggregates in an aqueous dispersion (Figure S14). Heating the aq CNC to 60 °C showed no significant change in the CD signal. Interestingly, CD signal was also observed in pure 1.0 wt % MC at 60 °C (Figure S14), possibly related to the existence of ring-like fibrillar structures.[47−49,51,52] Remarkably, CD signal was detected from MC/CNC gels at as low as 0.5 wt % of CNC in 1.0% MC. Further, the signals of MC/CNC were amplified by increasing CNC weight fractions as well as upon increasing the temperature. A temperature-dependent peak amplification and shift suggested possible structural deformations and the thermoresponsive nature of the CNC aggregates (Figure S14).

3.4. MC−CNC Interactions. In order to shed light on the inverse thermoreversible gelation and optical anisotropy, ITC was performed using MC/CNC 0.4 wt %/0.45 wt %, i.e., dilute concentrations, at 25 °C and upon heating to 60 °C, using MC14, MC41, and MC88. The titration curves and corresponding fits are shown in Figure 6 and Figure S15 for mixtures with different MC molecular weights. At 25 °C, the enthalpy change (ΔH) for the interaction of MC41 and CNC was negative (−3390 kcal/mol), whereas the entropic contribution ($-T\Delta S$) was almost the opposite (3369 kcal/mol), leading to a favorable net negative Gibbs free energy ($\Delta G = \Delta H - T\Delta S$) of −21 kcal/mol. For the other two MCs of different molecular weights, the findings were essentially similar at 25 °C (Figure S15), and the overall Gibbs free energy remained negative (−17 kcal/mol and −12 kcal/mol for MC88 and MC14, respectively), indicating attraction. Therefore, ITC suggests that CNC and MC spontaneously interact at room temperature, driven by enthalpic interactions tentatively based on hydrogen bonding and van der Waals interactions.

The situation drastically changes at 60 °C (Figure 6b and Figures S15). At this temperature, the enthalpy change was strongly positive (22630 kcal/mol for MC41), presumably highlighting the endothermic nature of the heat-induced MC gelation. The entropy factor ($-T\Delta S$) became strongly negative (−22654 kcal/mol), leading to a net negative Gibbs free energy change of −24 kcal/mol in the case of MC41/CNC. Therefore, at 60 °C, entropy was the driving force, but regardless of the change of the interaction of the components, the process remained spontaneous. Unfortunately, with the MC of the highest molecular weight MC88, the increased viscosity at 60 °C interfered with the measurements, making them less reliable. They gave only one reasonably coherent data set that produced a clearly deviating positive net ΔG of 67 kcal/mol. Nonetheless, the entropy-driven behavior appeared characteristic for all MC/CNC mixtures. Therefore, the roles of enthalpy and entropy completely overturned upon increasing the temperature. Positive enthalpic contribution due to gelation opposed the interaction, whereas entropic gain suggested hydrophobic interactions between MC and CNC and entropically favorable consequent structural adjustments of the fibrous MC, such as partial or local disassembly or release of water from the fibrils' solvation layer. This potentially contributes to the lack of visible fibrillar MC structures (TEM in Figure 2b). We also point out that all other samples, except those used in the ITC experiments, were prepared at room temperature, and the behavior at 60 °C was explored after the heating. Therefore, they were expected to involve history dependence upon heating, and the thermoreversible behavior can be more complex than suggested in the ITC experiments, where the samples were directly prepared at 60 °C.

3.5. Rationalization of the Results. Next, we suggest an explanation by combining our experimental observations and previous literature reports, see the schematics in Figure 7. First, as shown in Figure 1, MC chains at 20 °C exist in random coiled conformations. The chains are expected to be highly entangled as the concentration used in our experiments (1.0 wt % MC) is much above the overlap concentrations reported for methyl cellulose and other cellulose derivatives.[67] Further, it has been shown that the persistence length (L_p) for MC solutions at room temperature is ∼12−17 nm. Upon heating, the viscous fluid turns into a gel due to the formation of shape-persistent, long fibrils with ringlike lateral order and diameter of ∼14 nm (see Figure 1d, inset) as suggested by the previous models to explain the MC gelation at elevated temperatures[47−49,51,52] and supported by SEM of aerogels (Figure 4b). The temperature-dependent stiffening of pure MC gels also suggests a significant increase in L_p at higher temperature.[49] In MC/CNC composite hydrogels, the solid MC was added to the aqueous CNC dispersions; therefore, three possibilities can be assumed. First, when the concentration of CNC is below a critical concentration to induce gelation at room temperature, the adsorption of MC chains and

DOI: 10.1021/acs.biomac.8b00392
Biomacromolecules 2018, 19, 2795−2804

wrapping of CNCs is involved as reported in the literature (Figure 7a). However, because of more random coiling, the softer but entangled MC in this case leads to a smaller storage modulus. At small CNC aq concentrations, the CNCs have minimal mutual steric interactions, leading to reduced reinforcement (Figure 7a). Increasing the concentration above the percolation threshold, i.e, 1.5 wt % of CNCs led to rapid gelation at 20 °C, where MC chains interact enthalpically with CNCs as suggested by the ITC experiments. In this case, the CNCs exist as small chiral aggregates that are kinetically trapped within the MC network (Figure 7b), thus inducing some birefringence. At high temperature, MC/CNC gels showed increased storage modulus passing the percolation threshold at aq CNC 1.5 wt % with the fixed aq MC 1.0 wt % and creating a liquid crystalline order of CNC manifested as strong birefringence (Figure 7c). Note, however, that in MC/CNCs composite gels, the behavior of MC may be more complex than in the case of pure MC due to the interplay between CNC and MC. ITC suggests that, at high temperature, CNCs are entropically attracted to MC. SEM, TEM, and CD suggest that the birefringence is not due to nematic order but rather due to the chiral aggregates of CNC. Thus, CNC chiral aggregates can be expected to become topologically entrapped within the persistent fibrillar MC, thus effectively increasing the storage modulus.

4. CONCLUSIONS

Mixtures of MC and CNC form thermoreversible, tunable, and modular multifunctional bicomponent hydrogels where the liquid crystalline order and rheological properties can be tuned by temperature in a reversible manner. Using a fixed MC concentration of 1 wt % and varying the CNC loading in the range 0−3.5 wt % (below the critical LC concentration of pure aq CNC), and by controlling the temperature (20−70 °C), the rheological storage modulus is tunable in a range spanning almost three orders of magnitude. Upon increasing the CNC concentration past 1.0−1.5 wt %, the storage modulus of MC/CNC hybrids acquired a plateau, and the birefringence increased stepwise, suggesting a percolative phenomenon. Upon heating to 60−70 °C followed by recooling back to room temperature, the storage modulus and birefringence reversibly increased. The findings point toward reversible formation of CNC chiral aggregates, where the thermally induced space-filling aggregation within the gel network leads to stiffening. The findings suggest that detailed understanding of thermoreversible colloidal reinforcing filler and matrix interactions can allow unexpected new multiresponsive and functional biocomposites and thermosensitive biomaterials for future applications.

■ ASSOCIATED CONTENT

Supporting Information

The Supporting Information is available free of charge on the ACS Publications website at DOI: 10.1021/acs.biomac.8b00392.

Additional material regarding rheological properties, birefringence, conductometric titration data, dynamic light scattering data, zeta potential measurements, CD spectroscopy data, and ITC titration data (PDF)

■ AUTHOR INFORMATION

Corresponding Authors

*E-mail: nonappa@aalto.fi.
*E-mail: olli.Ikkala@aalto.fi.

ORCID

Sami Hietala: 0000-0003-1448-1813
Lasse Murtomäki: 0000-0001-7667-4325
Orlando J. Rojas: 0000-0003-4036-4020
Olli Ikkala: 0000-0002-0470-1889
Nonappa: 0000-0002-6804-4128

Notes

The authors declare no competing financial interest.

■ ACKNOWLEDGMENTS

Research technicians Marja Kärkkäinen and Tuyen Nguyen are acknowledged for their help in the preparation of CNCs and conductometric titrations, respectively. This work was carried out under the Academy of Finland Centre of Excellence Programme (HYBER 2014-2019) and supported by the ERC-Adv Grant (MIMEFUN 2012-2017 and DRIVEN 2017-2022) and Academy of Finland project 264677. V.H. acknowledges financial support from the Walter Ahlström Foundation. This work made use of the Aalto University Nanomicroscopy Center (Aalto-NMC) premises.

■ REFERENCES

(1) Habibi, Y.; Lucia, L. A.; Rojas, O. J. Cellulose Nanocrystals: Chemistry, Self-Assembly, and Applications. *Chem. Rev.* **2010**, *110* (6), 3479−3500.

(2) Marchessault, R. H.; Morehead, F. F.; Koch, M. J. Some Hydrodynamic Properties of Neutral Suspensions of Cellulose Crystallites as Related to Size and Shape. *J. Colloid Sci.* **1961**, *16* (4), 327−344.

(3) Revol, J.-F.; Bradford, H.; Giasson, J.; Marchessault, R. H.; Gray, D. G. Helicoidal Self-Ordering of Cellulose Microfibrils in Aqueous Suspension. *Int. J. Biol. Macromol.* **1992**, *14* (3), 170−172.

(4) Beck, S.; Méthot, M.; Bouchard, J. General Procedure for Determining Cellulose Nanocrystal Sulfate Half-Ester Content by Conductometric Titration. *Cellulose* **2015**, *22* (1), 101−116.

(5) Ureña-Benavides, E. E.; Ao, G.; Davis, V. A.; Kitchens, C. L. Rheology and Phase Behavior of Lyotropic Cellulose Nanocrystal Suspensions. *Macromolecules* **2011**, *44* (22), 8990−8998.

(6) Honorato-Rios, C.; Kuhnhold, A.; Bruckner, J. R.; Dannert, R.; Schilling, T.; Lagerwall, J. P. F. Equilibrium Liquid Crystal Phase Diagrams and Detection of Kinetic Arrest in Cellulose Nanocrystal Suspensions. *Front. Mater.* **2016**, *3*, 21.

(7) Revol, J.-F.; Godbout, L.; Dong, X.-M.; Gray, D. G.; Chanzy, H.; Maret, G. Chiral Nematic Suspensions of Cellulose Crystallites; Phase Separation and Magnetic Field Orientation. *Liq. Cryst.* **1994**, *16* (1), 127−134.

(8) Majoinen, J.; Kontturi, E.; Ikkala, O.; Gray, D. G. SEM Imaging of Chiral Nematic Films Cast from Cellulose Nanocrystal Suspensions. *Cellulose* **2012**, *19* (5), 1599−1605.

(9) Majoinen, J.; Hassinen, J.; Haataja, J. S.; Rekola, H. T.; Kontturi, E.; Kostiainen, M. A.; Ras, R. H. A.; Törmä, P.; Ikkala, O. Chiral Plasmonics Using Twisting along Cellulose Nanocrystals as a Template for Gold Nanoparticles. *Adv. Mater.* **2016**, *28* (26), 5262−5267.

(10) Dong, X. M.; Kimura, T.; Revol, J.-F.; Gray, D. G. Effects of Ionic Strength on the Isotropic-Chiral Nematic Phase Transition of Suspensions of Cellulose Crystallites. *Langmuir* **1996**, *12* (8), 2076−2082.

(11) Dong, X. M.; Gray, D. G. Effect of Counterions on Ordered Phase Formation in Suspensions of Charged Rodlike Cellulose Crystallites. *Langmuir* **1997**, *13* (8), 2404−2409.

(12) Beck-Candanedo, S.; Viet, D.; Gray, D. G. Induced Phase Separation in Low-Ionic-Strength Cellulose Nanocrystal Suspensions Containing High-Molecular-Weight Blue Dextrans. *Langmuir* **2006**, *22* (21), 8690−8695.

DOI: 10.1021/acs.biomac.8b00392
Biomacromolecules 2018, 19, 2795−2804

(13) Liu, D.; Wang, S.; Ma, Z.; Tian, D.; Gu, M.; Lin, F. Structure−color Mechanism of Iridescent Cellulose Nanocrystal Films. *RSC Adv.* **2014**, *4* (74), 39322−39331.
(14) Azzam, F.; Heux, L.; Jean, B. Adjustment of the Chiral Nematic Phase Properties of Cellulose Nanocrystals by Polymer Grafting. *Langmuir* **2016**, *32* (17), 4305−4312.
(15) Shopsowitz, K. E.; Qi, H.; Hamad, W. Y.; Maclachlan, M. J. Free-Standing Mesoporous Silica Films with Tunable Chiral Nematic Structures. *Nature* **2010**, *468*, 422−425.
(16) Dumanli, A. G.; Van Der Kooij, H. M.; Kamita, G.; Reisner, E.; Baumberg, J. J.; Steiner, U.; Vignolini, S. Digital Color in Cellulose Nanocrystal Films. *ACS Appl. Mater. Interfaces* **2014**, *6* (15), 12302−12306.
(17) Kelly, J. A.; Giese, M.; Shopsowitz, K. E.; Hamad, W. Y.; MacLachlan, M. J. The Development of Chiral Nematic Mesoporous Materials. *Acc. Chem. Res.* **2014**, *47* (4), 1088−1096.
(18) Shopsowitz, K. E.; Kelly, J. A.; Hamad, W. Y.; MacLachlan, M. J. Biopolymer Templated Glass with a Twist: Controlling the Chirality, Porosity, and Photonic Properties of Silica with Cellulose Nanocrystals. *Adv. Funct. Mater.* **2014**, *24* (3), 327−338.
(19) Guidetti, G.; Atifi, S.; Vignolini, S.; Hamad, W. Y. Flexible Photonic Cellulose Nanocrystal Films. *Adv. Mater.* **2016**, *28* (45), 10042−10047.
(20) Nan, F.; Chen, Q.; Liu, P.; Nagarajan, S.; Duan, Y.; Zhang, J. Iridescent Graphene/Cellulose Nanocrystal Film with Water Response and Highly Electrical Conductivity. *RSC Adv.* **2016**, *6* (96), 93673−93679.
(21) Zhang, H.; Jung, J.; Zhao, Y. Preparation and Characterization of Cellulose Nanocrystals Films Incorporated with Essential Oil Loaded β-Chitosan Beads. *Food Hydrocolloids* **2017**, *69*, 164−172.
(22) Zoppe, J. O.; Peresin, M. S.; Habibi, Y.; Venditti, R. A.; Rojas, O. J. Reinforcing Poly(ε-Caprolactone) Nanofibers with Cellulose Nanocrystals. *ACS Appl. Mater. Interfaces* **2009**, *1* (9), 1996−2004.
(23) Peresin, M. S.; Habibi, Y.; Zoppe, J. O.; Pawlak, J. J.; Rojas, O. J. Nanofiber Composites of Polyvinyl Alcohol and Cellulose Nanocrystals: Manufacture and Characterization. *Biomacromolecules* **2010**, *11* (3), 674−681.
(24) Cao, Y.; Zavaterri, P.; Youngblood, J.; Moon, R.; Weiss, J. The Influence of Cellulose Nanocrystal Additions on the Performance of Cement Paste. *Cem. Concr. Compos.* **2015**, *56*, 73−83.
(25) Ureña-Benavides, E. E.; Brown, P. J.; Kitchens, C. L. Effect of Jet Stretch and Particle Load on Cellulose Nanocrystal-Alginate Nanocomposite Fibers. *Langmuir* **2010**, *26* (17), 14263−14270.
(26) Liu, L.; Yao, J. M. Wet-Spinning of Reinforced Artificial Silk Hybrid Fibres by Cellulose Whiskers. *Adv. Mater. Res.* **2011**, *175−176*, 272−275.
(27) Ureña-Benavides, E. E.; Kitchens, C. L. Wide-Angle X-Ray Diffraction of Cellulose Nanocrystal−Alginate Nanocomposite Fibers. *Macromolecules* **2011**, *44* (9), 3478−3484.
(28) Dorris, A.; Gray, D. G. Gelation of Cellulose Nanocrystal Suspensions in Glycerol. *Cellulose* **2012**, *19* (3), 687−694.
(29) Ureña-Benavides, E. E.; Kitchens, C. L. Cellulose Nanocrystal Reinforced Alginate Fibers—Biomimicry Meets Polymer Processing. *Mol. Cryst. Liq. Cryst.* **2012**, *556* (1), 275−287.
(30) Zoppe, J. O.; Grosset, L.; Seppälä, J. Liquid Crystalline Thermosets Based on Anisotropic Phases of Cellulose Nanocrystals. *Cellulose* **2013**, *20* (5), 2569−2582.
(31) Chen, S.; Schueneman, G.; Pipes, R. B.; Youngblood, J.; Moon, R. J. Effects of Crystal Orientation on Cellulose Nanocrystals−Cellulose Acetate Nanocomposite Fibers Prepared by Dry Spinning. *Biomacromolecules* **2014**, *15* (10), 3827−3835.
(32) McKee, J. R.; Hietala, S.; Seitsonen, J.; Laine, J.; Kontturi, E.; Ikkala, O. Thermoresponsive Nanocellulose Hydrogels with Tunable Mechanical Properties. *ACS Macro Lett.* **2014**, *3* (3), 266−270.
(33) Way, A. E.; Hsu, L.; Shanmuganathan, K.; Weder, C.; Rowan, S. J. pH-Responsive Cellulose Nanocrystal Gels and Nanocomposites. *ACS Macro Lett.* **2012**, *1* (8), 1001−1006.
(34) Wilts, B. D.; Whitney, H. M.; Glover, B. J.; Steiner, U.; Vignolini, S. Natural Helicoidal Structures: Morphology, Self-Assembly and Optical Properties. *Mater. Today Proc.* **2014**, *1*, 177−185.
(35) Yaraghi, N. A.; Guarín-Zapata, N.; Grunenfelder, L. K.; Hintsala, E.; Bhowmick, S.; Hiller, J. M.; Betts, M.; Principe, E. L.; Jung, J.-Y.; Sheppard, L.; Wuhrer, R.; McKittrick, J.; Zavattieri, P. D.; Kisailus, D. A Sinusoidally Architected Helicoidal Biocomposite. *Adv. Mater.* **2016**, *28* (32), 6835−6844.
(36) Jativa, F.; Schütz, C.; Bergström, L.; Zhang, X.; Wicklein, B. Confined Self-Assembly of Cellulose Nanocrystals in a Shrinking Droplet. *Soft Matter* **2015**, *11* (26), 5374−5380.
(37) Li, Y.; Jun-Yan Suen, J.; Prince, E.; Larin, E. M.; Klinkova, A.; Thérien-Aubin, H.; Zhu, S.; Yang, B.; Helmy, A. S.; Lavrentovich, O. D.; Kumacheva, E. Colloidal Cholesteric Liquid Crystal in Spherical Confinement. *Nat. Commun.* **2016**, *7*, 12520.
(38) Parker, R. M.; Frka-Petesic, B.; Guidetti, G.; Kamita, G.; Consani, G.; Abell, C.; Vignolini, S. Hierarchical Self-Assembly of Cellulose Nanocrystals in a Confined Geometry. *ACS Nano* **2016**, *10* (9), 8443−8449.
(39) Wang, P.-X.; Hamad, W. Y.; MacLachlan, M. J. Structure and Transformation of Tactoids in Cellulose Nanocrystal Suspensions. *Nat. Commun.* **2016**, *7*, 11515.
(40) Kato, T.; Yokoyama, M.; Takahashi, A. Melting Temperatures of Thermally Reversible Gels IV. Methyl Cellulose-Water Gels. *Colloid Polym. Sci.* **1978**, *256* (1), 15−21.
(41) Miyamoto, T.; Takahashi, S.; Ito, H.; Inagaki, H.; Noishiki, Y. Tissue Biocompatibility of Cellulose and Its Derivatives. *J. Biomed. Mater. Res.* **1989**, *23* (1), 125−133.
(42) Kobayashi, K.; Huang, C.-I.; Lodge, T. P. Thermoreversible Gelation of Aqueous Methylcellulose Solutions. *Macromolecules* **1999**, *32* (21), 7070−7077.
(43) Desbrières, J.; Hirrien, M.; Ross-Murphy, S. B. Thermogelation of Methylcellulose: Rheological Considerations. *Polymer* **2000**, *41* (7), 2451−2461.
(44) Tate, M. C.; Shear, D. A.; Hoffman, S. W.; Stein, D. G.; LaPlaca, M. C. Biocompatibility of Methylcellulose-Based Constructs Designed for Intracerebral Gelation Following Experimental Traumatic Brain Injury. *Biomaterials* **2001**, *22* (10), 1113−1123.
(45) Funami, T.; Kataoka, Y.; Hiroe, M.; Asai, I.; Takahashi, R.; Nishinari, K. Thermal Aggregation of Methylcellulose with Different Molecular Weights. *Food Hydrocolloids* **2007**, *21* (1), 46−58.
(46) Chatterjee, T.; Nakatani, A. I.; Adden, R.; Brackhagen, M.; Redwine, D.; Shen, H.; Li, Y.; Wilson, T.; Sammler, R. L. Structure and Properties of Aqueous Methylcellulose Gels by Small-Angle Neutron Scattering. *Biomacromolecules* **2012**, *13* (10), 3355−3369.
(47) Bodvik, R.; Dedinaite, A.; Karlson, L.; Bergström, M.; Bäverbäck, P.; Pedersen, J. S.; Edwards, K.; Karlsson, G.; Varga, I.; Claesson, P. M. Aggregation and Network Formation of Aqueous Methylcellulose and Hydroxypropylmethylcellulose Solutions. *Colloids Surf., A* **2010**, *354* (1−3), 162−171.
(48) Lott, J. R.; McAllister, J. W.; Arvidson, S. A.; Bates, F. S.; Lodge, T. P. Fibrillar Structure of Methylcellulose Hydrogels. *Biomacromolecules* **2013**, *14* (8), 2484−2488.
(49) Lott, J. R.; McAllister, J. W.; Wasbrough, M.; Sammler, R. L.; Bates, F. S.; Lodge, T. P. Fibrillar Structure in Aqueous Methylcellulose Solutions and Gels. *Macromolecules* **2013**, *46* (24), 9760−9771.
(50) McAllister, J. W.; Schmidt, P. W.; Dorfman, K. D.; Lodge, T. P.; Bates, F. S. Thermodynamics of Aqueous Methylcellulose Solutions. *Macromolecules* **2015**, *48* (19), 7205−7215.
(51) Ginzburg, V. V.; Sammler, R. L.; Huang, W.; Larson, R. G. Anisotropic Self-Assembly and Gelation in Aqueous Methylcellulose-Theory and Modeling. *J. Polym. Sci., Part B: Polym. Phys.* **2016**, *54* (16), 1624−1636.
(52) Huang, W.; Ramesh, R.; Jha, P. K.; Larson, R. G. A Systematic Coarse-Grained Model for Methylcellulose Polymers: Spontaneous Ring Formation at Elevated Temperature. *Macromolecules* **2016**, *49* (4), 1490−1503.
(53) Roman, M.; Dong, S.; Hirani, A.; Lee, Y. W. Cellulose Nanocrystals for Drug Delivery. *ACS Symp. Ser.* **2010**, *1017*, 81−91.

DOI: 10.1021/acs.biomac.8b00392
Biomacromolecules 2018, 19, 2795−2804

(54) Modulevsky, D. J.; Cuerrier, C. M.; Pelling, A. E. Biocompatibility of Subcutaneously Implanted Plant-Derived Cellulose Biomaterials. *PLoS One* **2016**, *11* (6), e0157894.
(55) Kontturi, E.; Laaksonen, P.; Linder, M. B.; Nonappa; Gröschel, A. H.; Rojas, O. J.; Ikkala, O. Advanced Materials through Assembly of Nanocelluloses. *Adv. Mater.* **2018**, 1703779.
(56) Hu, Z.; Xia, X. Hydrogel Nanoparticle Dispersions with Inverse Thermoreversible Gelation. *Adv. Mater.* **2004**, *16* (4), 305−309.
(57) Hu, Z.; Xu, R.; Cranston, E. D.; Pelton, R. H. Stable Aqueous Foams from Cellulose Nanocrystals and Methyl Cellulose. *Biomacromolecules* **2016**, *17* (12), 4095−4099.
(58) Kedzior, S. A.; Dubé, M. A.; Cranston, E. D. Cellulose Nanocrystals and Methyl Cellulose as Costabilizers for Nanocomposite Latexes with Double Morphology. *ACS Sustainable Chem. Eng.* **2017**, *5* (11), 10509−10517.
(59) Rivkin, A.; Abitbol, T.; Nevo, Y.; Verker, R.; Lapidot, S.; Komarov, A.; Veldhuis, S. C.; Zilberman, G.; Reches, M.; Cranston, E. D.; Shoseyov, O. Bionanocomposite Films from Resilin-CBD Bound to Cellulose Nanocrystals. *Ind. Biotechnol.* **2015**, *11* (1), 44−58.
(60) Edgar, C. D.; Gray, D. G. Smooth Model Cellulose I Surfaces from Nanocrystal Suspensions. *Cellulose* **2003**, *10* (4), 299−306.
(61) Lokanathan, A. R.; Uddin, K. M. A.; Rojas, O. J.; Laine, J. Cellulose Nanocrystal-Mediated Synthesis of Silver Nanoparticles: Role of Sulfate Groups in Nucleation Phenomena. *Biomacromolecules* **2014**, *15* (1), 373−379.
(62) Schindelin, J.; Arganda-Carreras, I.; Frise, E.; Kaynig, V.; Longair, M.; Pietzsch, T.; Preibisch, S.; Rueden, C.; Saalfeld, S.; Schmid, B.; Tinevez, J. Y.; White, D. J.; Hartenstein, V.; Eliceiri, K.; Tomancak, P.; Cardona, A. Fiji: An Open-Source Platform for Biological-Image Analysis. *Nat. Methods* **2012**, *9* (7), 676−682.
(63) Schneider, C. A.; Rasband, W. S.; Eliceiri, K. W. NIH Image to ImageJ: 25 Years of Image Analysis. *Nat. Methods* **2012**, *9* (7), 671−675.
(64) Lagerwall, J. P. F.; Schütz, C.; Salajkova, M.; Noh, J.; Hyun Park, J.; Scalia, G.; Bergström, L. Cellulose Nanocrystal-Based Materials: From Liquid Crystal Self-Assembly and Glass Formation to Multifunctional Thin Films. *NPG Asia Mater.* **2014**, *6* (1), e80.
(65) Ferry, J. D. *Viscoelastic Properties of Polymers*, 3rd ed.; John Wiley & Sons: New York, 1980.
(66) Liu, Q.; Smalyukh, I. I. Liquid Crystalline Cellulose-Based Nematogels. *Sci. Adv.* **2017**, *3* (8), e1700981.
(67) El Ghzaoui, A.; Trompette, J. L.; Cassanas, G.; Bardet, L.; Fabregue, E. Comparative Rheological Behavior of Some Cellulosic Ether Derivatives. *Langmuir* **2001**, *17* (5), 1453−1456.

DOI: 10.1021/acs.biomac.8b00392
Biomacromolecules 2018, 19, 2795−2804